Applied Catalysis B: Environmental 324 (2023) 122263

Contents lists available at ScienceDirect

Applied Catalysis B: Environmental

journal homepage: www.elsevier.com/locate/apcatb

Understanding the temperature-dependent H_2O promotion effect on SO_2 resistance of MnO_x-CeO_2 catalyst for SCR denitration

Jiawei Ji [a], Ningze Gao [a], Wang Song [a], Yu Tang [a], Yandi Cai [b], Li Han [a], Lijun Cheng [c], Jingfang Sun [e], Shenggui Ma [d,*], Yinghao Chu [d], Changjin Tang [c,*], Lin Dong [a,b,e,**]

[a] Laboratory of Mesoscopic Chemistry of MOE, School of Chemistry and Chemical Engineering, Nanjing University, Nanjing 210023, PR China
[b] School of the Environment, Nanjing University, Nanjing 210023, PR China
[c] Jiangsu Province Engineering Research Center of Environmental Risk Prevention and Emergency Response Technology, School of Environment, Nanjing Normal University, Nanjing 210023, PR China
[d] College of Architecture and Environment, National Engineering Research Center for Flue Gas Desulfurization, Sichuan University, Chengdu 610065, PR China
[e] Jiangsu Key Laboratory of Vehicle Emission Control, Center of Modern Analysis, Nanjing University, Nanjing 210023, PR China

ARTICLE INFO

Keywords:
MnO_x-CeO_2 catalyst
Ultra-low temperature denitration
SO_2 resistance
H_2O promotion
Sulfite species

ABSTRACT

Understanding how H_2O affects SO_2 tolerance of SCR catalysts at different working temperatures is of great importance. Herein, we reported that H_2O addition at ultra-low temperature of 100 °C induced a significant promotion on SO_2 tolerance of MnO_x-CeO_2 catalysts. Sole SO_2 led to serious activity loss from 100% to 20%, while H_2O coexistence alleviated the deactivation and an admirable activity of 60% was reserved. Combining experimental characterizations with DFT calculation, we demonstrated that H_2O promoted hydroxyl formed on defect sites, which promoted more sulfite formation and retarded sulfates with strong electron-withdrawing capacity disturbing active Mn sites. In comparison with sulfates, sulfites exhibited less interference in adsorbed species, ensuring the occurrence of Eley-Rideal and Langmuir-Hinshelwood mechanisms. The present study discloses the unique temperature-dependent effect of H_2O on SO_2 tolerance, which is expected to deepen our understanding on the role of H_2O in modulating surface species and catalytic behaviors of SCR catalysts.

1. Introduction

Selective catalytic reduction (SCR) of environmentally harmful nitrogen oxides (NO_x) with NH_3 is a proven technology for the denitrification of exhaust gases from stationary sources [1,2]. Commercial catalysts with the chemical composition of V_2O_5-$WO_3(MoO_3)/TiO_2$ exhibit high catalytic performance and superior SO_2/H_2O resistance in the operating temperature window of 300–420 °C, making them rather effective in the treatment of NO_x effluents from coal-fired power plants [3]. Despite the great success in thermal power stations, the control of NO_x in non-electric industries remains a formidable challenge, mainly due to the aggravated disturbing effect from SO_2 and H_2O caused by lower operating temperatures [4,5]. At the typical low working temperatures (80–200 °C) [6,7], V_2O_5-$WO_3(MoO_3)/TiO_2$ falls short of providing sufficient performance. Therefore, it is very urgent to develop SCR catalysts with splendid denitration efficiency and good SO_2/H_2O tolerance at this temperature range.

Understanding detailed SO_2 and H_2O poisoning mechanisms are crucial to the development of well-performed SCR catalysts for practical application. Tremendous efforts have been made to explore the deactivation mechanisms of SCR catalysts in the presence of SO_2. Normally, SO_2 poisoning of SCR catalysts can be segmented into two aspects, *i.e.*, the sulfation of active metal sites and the deposition of ammonium sulfates salts [6,8]. Xu et al. found that the main deactivation reason for V_2O_5-WO_3/TiO_2 was the formation of NH_4HSO_4, while both cerium sulfates and NH_4HSO_4 accounted for the deactivation of CeO_2-WO_3/TiO_2 [9]. Additionally, the influence of H_2O on SCR catalysts is also explored. The effect of H_2O is always reported to be inhibitory, including irreversible deactivation *via* the occupation of active sites and reversible competitive adsorption [10]. Kijlatra et al. employed γ-Al_2O_3-supported manganese oxides to study the poisoning effect of H_2O and found that both the reversible and irreversible deactivation happened after the

* Corresponding authors.
** Corresponding author at: Laboratory of Mesoscopic Chemistry of MOE, School of Chemistry and Chemical Engineering, Nanjing University, Nanjing 210023, PR China.
E-mail addresses: masgui@scu.edu.cn (S. Ma), tangcj@njnu.edu.cn (C. Tang), donglin@nju.edu.cn (L. Dong).

https://doi.org/10.1016/j.apcatb.2022.122263
Received 12 September 2022; Received in revised form 3 November 2022; Accepted 3 December 2022
Available online 5 December 2022

introduction of H_2O. The deactivation from H_2O could be partially reversed after removal, suggesting the simultaneous occurrence of irreversible deactivation. They further proposed the unrecovered reaction rate (irreversible part) mainly resulted from the formation of surface hydroxyl species, which could be regenerated after high-temperature treatment [11].

Although the poisoning mechanisms of SO_2 and H_2O alone have been investigated comprehensively, the combined effect of SO_2 and H_2O coexistence still lacks sufficient study, especially at ultra-low temperatures (<150 °C). In actual operation conditions of non-electric industries, the denitrification unit is always placed in the down-stream of dust removal and desulphurization units to remove toxic components [6, 12], which can result in a further decrease of exhaust temperature to around 100 °C. To avoid the energy consumption caused by flue gas reheating, it is of great significance to develop SCR catalysts to satisfy the demand in such a temperature range. However, limited by the poor tolerance of SCR catalysts to SO_2 or H_2O alone at this temperature, little information can be found in the literature regarding the reaction behavior of SCR catalysts under SO_2 and H_2O coexistence.

Herein, MnO_x-CeO_2 catalysts (MnCe) with a good catalytic performance at ultra-low temperature were employed as a model for investigation. Surprisingly, a novel phenomenon related to the H_2O promotion effect on alleviating SO_2 poisoning at 100 °C was found. Through comprehensive quantitative analysis and DFT simulation, it was found that the introduction of H_2O suppressed the electron interaction between surface Mn and sulfur species *via* hydroxyl modulation, making a prominent contribution to the formation of more sulfites on MnCe catalyst. *In situ* DRIFTS and kinetics analysis were performed to investigate the distinct effects of sulfate and sulfite species on the adsorption properties and reaction mechanism, through which the reasons for the unusual enhancement in SO_2 resistance by H_2O at ultra-low temperature were revealed in depth.

2. Materials and methods

2.1. Preparation of catalysts

A conventional co-precipitation method was employed to prepare MnO_x-CeO_2 catalysts. Typically, 0.0217 mol $(NH_4)_2Ce(NO_3)_6$ and 0.0145 mol $Mn(NO_3)_2{\cdot}9H_2O$ were dissolved in 150 mL deionized H_2O with successive stirring. 25% concentration of $NH_3{\cdot}H_2O$ was employed as a precipitant and dripped slowly into the solution using a dropper under stirring till the pH level reached 10. After that, the obtained solution was aged in the beaker overnight in the fume hood, followed by filtrating and washing using deionized water five times. Then, the resulting solid was dried in an oven at a setting temperature of 100 °C for 12 h and finally calcined in the muffle furnace at 550 °C for 240 min (2 °C/min as the ramping rate). For the sake of simplicity, the obtained sample was marked as MnCe.

MnCe with different poisoning conditions was treated under the reaction atmosphere containing SO_2 or $SO_2 + H_2O$. In the actual test, fresh MnCe (100 mg, 40–60 mesh) was preheated in Ar stream at a setting temperature of 200 °C for half an hour. After cooling down to the reaction temperature (100 °C), the mixed gases (500 ppm NO, 500 ppm NH_3, 100 ppm SO_2, 5 *vol.*% O_2, 5–15% H_2O (when needed), and balanced with Ar) were switched on and kept reaction for 9 h. The reacted catalysts were marked with MnCe-SO_2+*x*%H_2O (x = 0, 5, 10, 15).

2.2. Catalyst characterization

N_2 adsorption-desorption tests were measured to test specific surface area at −196 °C employing the adsorption instrument (Micromeritics ASAP-2020). Prior to the measurement, MnCe catalysts were degassed at 80 °C under a stable vacuum for 3 h.

The crystalline structure information of prepared MnCe catalysts was recorded by powder X-ray diffraction (XRD) on a diffractometer instrument (Philips X′pert Pro) employing Cu K_α radiation ($\lambda = 0.154056$ nm). 2θ was ranged from 20.0 to 60.0° (10.0°/min as scan speed and 0.02° as step size).

Surface species on MnCe after the anti-sulfur test were tested using ion chromatography (IC) on DX-120 (DIONEX). Before test, 10 mg catalyst was dissolved under sonication in deionized water of 5 mL mixed with 0.3 mL nitric acid solution (16 mol/L).

The X-ray photo-electron spectroscopy (XPS) was recorded on Scanning X-ray Microprobe (PHI 5000 Versa Probe), where a monochromatized Al K_α X-ray (1486.6 eV, 15 kW) source was equipped. The C *1s* (284.8 eV) signal of exogenous carbon was used to be the reference for all elements.

High-resolution transmission electron microscopy (HR-TEM) was measured on JEM-2100. Before tests, the MnCe catalysts were ultrasonically dispersed in ethyl alcohol for 60 min. A drop of suspension was roasted over a copper grid supporting carbon membrane.

NH_3 and NO temperature-programmed desorption (NH_3-TPD and NO-TPD) were carried out using a FT-IR spectrometer (Nicolet IS-10) to detect the gas composition, which was equipped with a gas cell (multiple-path, 2 m). Tested samples were placed into a quartz reactor (0.5 cm for inner diameter) in a flow of 100 mL/min. A 100 mg amount of sample was exposed to specific reaction atmosphere at 100 °C for saturation. Then, the catalysts were flushed by Ar. All TPD tests were recorded in the temperature ranges from reaction temperature to 600 °C (10 °C/min for heating rate).

The reduction property of catalyst was evaluated *via* temperature-programmed reduction with H_2 (H_2-TPR) employing the U-tube reactor, which was equipped with a thermal conduct detector (TCD). 7 *vol.*% H_2/Ar was used to be the reductant. In a typical test, 10 mg catalyst was precisely weighted for the TPR measurement. Prior to switching to H_2 reduction, the catalyst was preheated in an inert nitrogen flow to 80 °C for an hour. The TCD signal was recorded from 50 °C to 800 °C linearly (10 °C/min as heating rate).

The oxidization property of catalysts was tested *via* O_2 temperature-programmed desorption (O_2-TPD) in a fixed bed reactor with the steady-state flow, using a quadrupole mass-spectrometer to trace O_2 signal. For this, 100 mg sample was weighted and exposed to 5% O_2 (Ar in balance) for 60 min at 100 °C. Thereafter, excessive physisorbed or weakly species were removed using Ar for another 1 h. The desorbed O_2 signal was collected in a range from 100 to 600 °C (10 °C/min as a heating rate).

In situ diffuse reflectance infrared Fourier transformed spectra (DRIFTS) were performed on Nicolet-5700. The spectrometer was assembled with a mercury cadmium telluride (MCT) detector, using liquid N_2 to cool down (−196 °C). The scan number during the experiment was set to be 32 from 400 to 4000 cm^{-1} with 4 cm^{-1} in resolution. Before each test, the sample loaded in the reaction cell (HARRICK, containing ZnSe windows) was flattened carefully with the aim to strengthen reflection signal.

2.3. Activity measurement

NH_3-SCR reaction performances were tested using 100 mg catalysts (40–60 mesh) in the fixed-bed reactor, using a FT-IR spectrometer (Nicolet IS-10). The feed gas consisted of 500 ppm NO, 500 ppm NH_3, 5 *vol.*% O_2, 5–15% H_2O (when needed), 100 ppm SO_2 (when needed), and Ar balance to 100 mL/min. The concentration remaining in the exhaust (NO, NO_2, N_2O, and NH_3) was monitored after keeping the temperature stable for 0.5 h. NO conversion (Con_{NO}) along with N_2 selectivity (Sel_{N2}) was calculated according to the equations attached:

$$Con_{NO}(\%) = \frac{C_{NO,in} - C_{NO,out}}{C_{NO,in}} \times 100\%$$

$$Sel_{N_2}(\%) = \frac{C_{NO,in} - C_{NO,out} + C_{NH_3,in} - C_{NH_3,out} - C_{NO_2,out} - 2C_{N_2O,out}}{C_{NO,in} - C_{NO,out} + C_{NH_3,in} - C_{NH_3,out}} \times 100\%$$

2.4. Kinetics test

Kinetics measurement was conducted in a similar condition to the activity test. NO conversion rate was limited below 30% to be within the kinetic range. Detailed eliminations of internal and external diffusions were presented in Fig. S1 and Fig. S2. Feed gas was composed with 100–500 ppm NO, 100–500 ppm NH_3, 5 *vol.*% O_2, 10% H_2O, and Ar balance to 100 mL/min. 10 mg catalyst was diluted using 90 mg carborundum (SiC). The weight hourly space velocity (WHSV) was calculated to be 600,000 $mL{\cdot}h^{-1}{\cdot}g^{-1}$. Reaction rates (r) were evaluated using the equations below:

$$r = \frac{v \times \alpha}{V_m \times m}$$

here, v ($m^3{\cdot}min^{-1}$) is the NO flow rate, α (%) represents for the NO conversion, V_m ($m^3{\cdot}mol^{-1}$) refers to the gas molar constant, and m (g) stands for the catalyst mass.

2.5. Computational details

Spin-polarized density functional theory (DFT) calculations were carried out by Vienna *ab initio* simulation package (VASP) code [13], employing projector-augmented wave (PAW) method. A DFT + U method was applied to Ce *4f* and Mn *3d* states with the effective values (U-J) of 5.0 and 4.5 eV, to describe the strong on-site Coulomb interactions [14]. The *van der Waals* correction was considered employing the DFT-D3 raised by Grimme. The exchange-correlation energy was expressed in the general gradient approximation and Perdew-Burke-Ernzerhof exchange-correlation functional and (GGA-PBE). The plane-wave basis set with an energy cut-off of 450 eV was employed in the work. Numerical integration in the first Brillouin zone is carried out using a Monkhorst-Pack grid of 3 × 3 × 1 for surface models. All the energy of the system converges to 1×10^{-6} eV. And the force on each atom is less than 0.01 eV/Å. The transition states (TS) were searched using a method combining a climbing image-nudged elastic band (CI-NEB) method and dimer method.

3. Result and discussion

3.1. Catalytic performance and SO_2 resistance

To obtain an optimal MnO_x-CeO_2 SCR catalyst, the initial screening of catalysts was carried out through ratio regulation. As shown in Fig. S3, an optimized MnCe catalyst with a ratio of 4:6 exhibited the best NH_3-SCR activity, which was in line with the work by R. T. Yang [15]. And this optimized ratio of MnCe catalyst was employed in the subsequent study.

The SCR performance on MnCe catalysts in terms of NO conversion, N_2 selectivity, and SO_2/H_2O resistance was first explored. As shown in Fig. 1a, MnCe exhibited excellent SCR performance at low temperature, which was revealed by the acquirement of 80% NO conversion at 75 °C and full NO conversion in the temperature range of 100–200 °C. With the addition of moderate H_2O (10% in volume percentage), a distinct inhibition effect on NO conversion was observed, particularly at the temperature range between 50 and 100 °C, which could be reasonably ascribed to the competitive adsorption of NH_3 and NO_x with H_2O at ultra-low temperatures [16,17]. This result indicated that H_2O acted as toxic species in SCR reaction on MnCe catalysts. As for N_2 selectivity, H_2O played a decisive role in restraining the formation of byproducts (Fig. S4), in line with the previous report that N_2O generation could be controlled by H_2O due to the suppression of NH_4NO_3 formation [18]. On the other hand, SO_2 tolerance at 100 °C was evaluated and corresponding results were presented in Fig. 1b. It was found that with the 100 ppm SO_2 introduction, NO conversion decreased sharply from 100% to only 20% after successive reaction of 9 h, suggesting serious deactivation caused by SO_2 at ultra-low temperature.

Interestingly, when 10% H_2O was added to the above reaction stream, no further deactivation was detected. Instead, an obvious promotion in activity was exhibited, as could be evidenced by the obtainment of an admirable NO conversion value of 60% after the continuous test of 9 h. To further explore the effect of H_2O content, 5% and 15% H_2O were introduced into the reaction stream. For the case containing 5% H_2O, 40% NO conversion was obtained after a 9 h test. This efficiency was a little lower than that with 10% H_2O but still higher than the case merely with SO_2, verifying that H_2O addition was indeed effective in improving SO_2 resistance. As for the condition of 15% H_2O, some difference was exhibited. Approximate the same NO conversion was achieved with that of 5% H_2O, which appeared to display an inverse trend. However, it was worth noting that when 15% H_2O was added, a sharp decrease in NO conversion from 100% to 60% was accomplished in 1 h and after that, a gradual decline of activity to 40% was detected in the following 8 h. According to the literature, the rapid deactivation in the first hour might comprise the severe competitive adsorption between reactant molecules and excessive H_2O [19,20]. Thus, the deactivation rate under 15% H_2O was calculated based on the deactivation profile after the first hour. The result was presented in Fig. 1**c** and it was found the deactivation effect was gradually alleviated as the amount of H_2O increased. Based on the above results, the novel effect of H_2O addition in upgrading the SO_2 resistance of MnCe catalyst was confirmed.

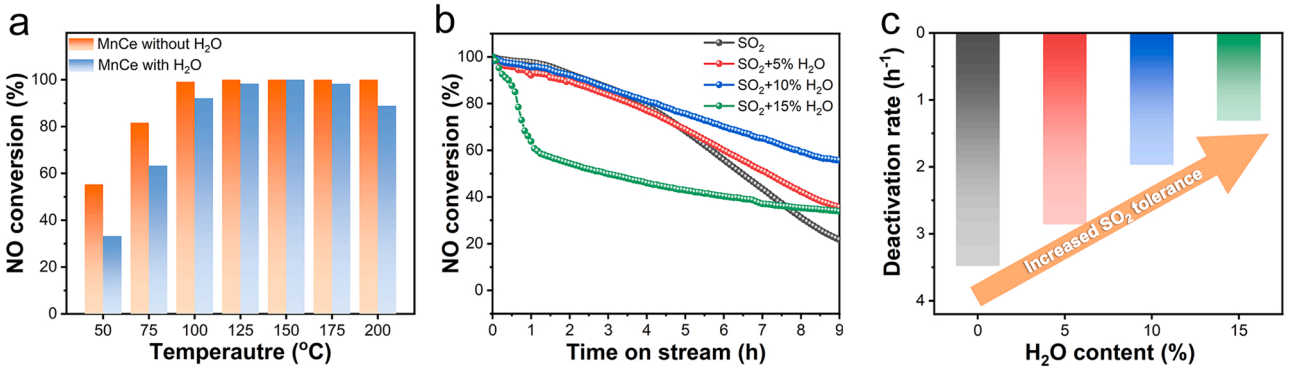

Fig. 1. (a) NO conversion over MnCe in the absence and presence of H_2O; (b) SO_2 resistance and (c) deactivation rate over MnCe under different H_2O contents at 100 °C. Test condition: 500 ppm NO, 500 ppm NH_3, 5 *vol.*% O_2, 100 ppm SO_2 (when needed), 5–15% H_2O (when needed), and Ar balance, WHSV = 60,000 $mL{\cdot}g^{-1}{\cdot}h^{-1}$. Deactivation rates of the MnCe-SO_2, MnCe-SO_2+5%H_2O, and MnCe-SO_2+10%H_2O were obtained by linear fits of 0–9 h activity profiles and that of the MnCe-SO_2+15%H_2O were calculated based on 1–9 h anti-SO_2 profile.

It is well known that SO_2 and H_2O are widely present in industrial flue gas, and there are lots of studies investigating the deactivation mechanism under SO_2 and H_2O coexistence at temperature higher than 150 °C. As can be seen from Fig. 2 (detailed test conditions were compiled in Table S1 in Supplementary Materials), despite the varied extent of activity change, it is clear that the addition of H_2O always poses a detrimental effect on SO_2 poisoning of SCR catalysts, which is much different from the observation in the present study. Additionally, we found the promotion effect was not exclusive to the MnO_x-CeO_2 catalyst. Pure MnO_x and other Mn-based catalysts (*i.e.,* MnCo and MnCoSn) displayed a similar behavior at 100 °C (Figs. S5-S6). As such, we suppose the novel effect might be related to the different reaction temperature ranges. To check this point, the SO_2 resistance of MnO_x-CeO_2 catalysts at a higher temperature of 200 °C was explored. At this time, we found the result was in line with conventional report and H_2O addition speeded up SO_2 deactivation rate. As shown in Fig. S7, the activity of MnCe fell from 100% to 63% under dry operation conditions, while wet conditions gave a much lower value of 36%. Nevertheless, when the operating temperature was reduced to below 150 °C, the alleviating effect of H_2O against SO_2 poisoning was much enhanced with the decrease of temperature. Remarkably, it could even retain a stable NO conversion of *ca.*40% at 75 °C under SO_2 and H_2O coexistence (Fig. S8). This result depicted a temperature-dependent effect from H_2O on SO_2 tolerance of SCR catalysts. To uncover the origin of H_2O addition in promoting SO_2 resistance of MnCe catalyst at ultra-low temperature, diverse characterizations were performed.

3.2. Characterization of phase structure and textural property

To ascertain any disturbance from reaction atmospheres on the crystalline structure of MnCe catalyst, the XRD patterns of fresh and poisoned MnCe catalysts were collected. As presented in Fig. 3, no diffraction peaks for MnO_x were observed for fresh MnCe catalyst, and the typical diffraction peaks at 2θ = 28.5, 33.1, 47.5, and 56.3° was filed into the (111), (200), (220), and (311) crystal planes of cubic fluorite CeO_2 (PDF-ICDD 34–0394). After the reaction, negligible modification of XRD profiles was observed (Fig. 3b), suggesting that the addition of H_2O in reaction atmosphere did not induce an apparent change in the crystalline structure. Moreover, no diffraction peaks ascribed to sulfur species were observed, indicating the absence of bulk or bulk-like sulfur species. Sulfur species were highly dispersed or existed as small particles on the surface of MnCe catalysts [8].

In addition to phase structure, the catalytic performance of SCR catalysts can also be potentially affected by the alteration of textural properties. This is particularly true for SO_2 resistance since one important reason for SO_2 deactivation comes from the decrease in surface area induced by sulfur species deposition on the catalyst [5,6]. To explore this possibility, the specific surface area of fresh and poisoned catalysts

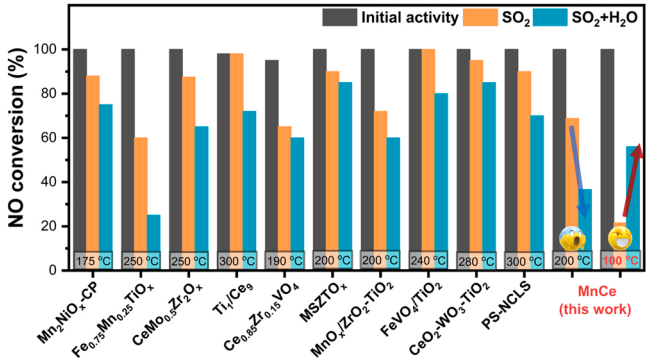

Fig. 2. A literature survey of reported anti-SO_2/SO_2+H_2O performance on various SCR catalysts and the direct comparison with the test results on MnCe catalysts at different temperature points.

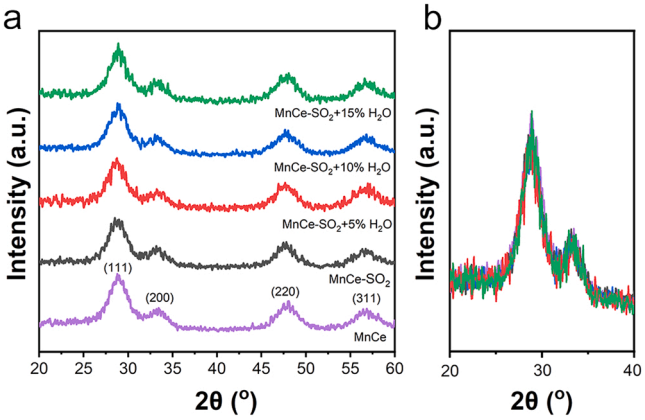

Fig. 3. The XRD pattern of fresh and poisoned MnCe.

with different H_2O contents was measured through N_2-sorption (Table 1). Original MnCe presented an admirable surface area of 133.5 m^2/g. However, this value decreased significantly to 51.1 m^2/g after the SO_2 resistance test under dry condition. Moreover, a further reduction of surface area was detected with H_2O introduction, and it actually displayed a monotonous relation with H_2O content. Given that no obvious change was shown by XRD on MnCe catalysts, the contribution from growth of ceria size was excluded. As such, the decrease in specific surface area was reasonably ascribed to the sulfur species deposition on the MnCe surface [21,22]. Nevertheless, no clear relationship could be constructed to explain the deactivation behavior regarding the change of surface area. Therefore, it is supposed that the reduction in surface area was not the dominant reason for activity change in the presence of SO_2 and H_2O.

3.3. Exploration of sulfur species

The result of N_2-sorption suggested the existence of deposited sulfur species on MnCe surface. The accelerated deposition of sulfur species resulting from H_2O addition is generally considered to be the origin of aggravated deactivation. Wijayanti et al. found the content of deposited sulfur species increased from 0.4 *wt.*% to 1.4 *wt.*% after H_2O addition at 200 °C on Cu-SSZ-13 [23]. Therefore, XRF characterization was carried out to quantify the amount of sulfur species. As shown in Table 1, the content of sulfur species was measured to be 9.56 *wt.*% for the MnCe-SO_2 sample. When different amount of H_2O was added along with SO_2, the sulfur concentration kept almost the same. In addition, the EDS-mapping result showed that sulfur species were dispersed on MnCe catalysts and no obvious aggregation of S was observed (Fig. S9), which was also supported by surface element analysis *via* XPS (Table S2). This result excluded the influence from deposition amount and dispersion condition of sulfur species on the deactivation behavior of MnCe catalyst.

The variation of surface sulfur species was further distinguished by ion chromatography (IC) and the results were summarized in Table 1.

Table 1
Texture property and quantitative results of XRF, ion chromatography, and XPS.

Sample	BET surface (m^3/g)	S content (*wt.*%)	SO_3^{2-} ratio (%)
MnCe	133.5	/	/
MnCe-SO_2	51.1	9.56[a]/ 9.93[b]	10.57[b]/ 16.03[c]
MnCe-SO_2+5%H_2O	41.4	9.67[a]/ 9.98[b]	18.24[b]/ 31.70[c]
MnCe-SO_2+10%H_2O	33.4	9.45[a]/ 9.84[b]	25.10[b]/ 39.04[c]
MnCe-SO_2+15%H_2O	29.7	9.51[a]/ 9.83[b]	27.06[b]/ 46.49[c]

[a] Measured result from XRF.
[b] Measured result from ion chromatography, detailed concentrations were listed in Table S3.
[c] Measured result from XPS.

Both sulfates and sulfites were detected over SO_2 poisoned MnCe. The calculation of total sulfur species by summing up sulfates and sulfites showed almost the same value around 9.90 *wt.*% for all poisoned catalysts, which was compatible with XRF results. As for the distribution of diverse sulfur species, it differed significantly with H_2O content. It is obvious that sulfates species were dominant and sulfite species only accounted for 10.57% on MnCe-SO_2. With the addition of H_2O content from 5% to 15%, the SO_3^{2-} ratio exhibited a significant increase from 18.24% to 27.0%, suggesting the obvious promotion effect of H_2O on sulfite formation.

The presence of sulfite and sulfate species on MnCe catalysts was also disclosed by XPS characterization and the result was shown in Fig. 4a. Two pairs of doublets over S *2p* were deconvolved, where the criteria for deconvolution are intensity ratio of 0.511 and ΔBE (binding energy) of 1.18 eV between S $2p_{1/2}$ and $2p_{3/2}$ spin-orbit states [24]. As summarized in Table 1, sulfates dominated the total sulfur species on MnCe-SO_2 and sulfite species only accounted for 16.03%. In the case of MnCe-SO_2+5% H_2O, the proportion of sulfites significantly increased to 31.70%, almost twice that of MnCe-SO_2. With the H_2O content further increasing to 10% and 15%, the percentage of sulfites was fortified to 39.04% and 46.49%, respectively.

Based on the characterization results of XRF, IC, and XPS, it is confirmed that the addition of H_2O hardly affected the deposited amount of sulfur species, but indeed restricted SO_2 oxidation at the temperature as low as 100 °C. As could be noted from Fig. 4b, there appeared a certain correlation between the deactivation rate and sulfite content. Moreover, when MnCe catalyst was reacted at a higher temperature of 200 °C, the XPS signal around 167.9 eV for sulfites could no longer be detected (Fig. S10), suggesting the exclusive presence of sulfur species as sulfates. In that case, the aggravated deactivation from H_2O might result from the accelerated deposition of sulfate species (Fig. S7) [25,26]. Taking this point into consideration, it is reasonable to propose that the formation of sulfites accounted for the main reason for the alleviated SO_2 poisoning with the introduction of H_2O at ultra-low temperature.

3.4. Surface properties of MnCe catalysts

To learn more about the effect of H_2O addition on the interaction between SO_2 and MnCe catalyst, MnCe-SO_2 and MnCe-SO_2+10%H_2O after poisoned in SCR reaction atmosphere were selected as representatives for further analysis. Additionally, unless otherwise specified, MnCe-SO_2+H_2O was used to represent MnCe-SO_2+10%H_2O for simplicity in the follow-up study.

XPS was used to explore the surface electronic states of fresh and poisoned catalysts. Ce *3d* spectra were deconvolved and filed in Fig. 5a. Typically, two doublets for Ce^{3+} and three doublets for Ce^{4+} are fitted for Ce *3d*, which are related to the initial states of $3d^{10}4f^1$ and $3d^{10}4f^0$ and various final states caused by the transitions from the valance band electrons to Ce *4f* states [27]. The concentration of Ce^{3+} can be calculated based on the following equation:

$$Ce^{3+}(\%) = \frac{S_{u^0} + S_{v^0} + S_{u'} + S_{v'}}{\sum (S_u + S_v)} \times 100\%$$

As directly summarized in Fig. 5a, the Ce^{3+} ratio of pristine MnCe was 12.70% and it increased to 18.09% after the exposure to the reaction stream containing SO_2. With the coexistence of SO_2 and H_2O in SCR atmosphere, the Ce^{3+} kept almost the same value of 18.16%. For the Mn signal (Fig. 5b), Mn *2p* spin-orbital coupling peaks composed of two subpeaks corresponding to Mn^{3+} (641.4–641.9 eV) and Mn^{4+} (641.9–643.0 eV) were presented [28]. The initial Mn^{3+} of MnCe was calculated to be 42.67% based on the integral area. For MnCe-SO_2, the ratio of Mn^{3+} increased to 55.78%. As a comparison, Mn^{3+} content exhibited a minor growth to 46.88% for MnCe-SO_2+H_2O. The surface valence changes of Mn species were additionally reflected by Mn *3s* spectra (Fig. S11). The magnitude of two multiplets split components caused by the coupling of non-ionized *3s* electron and *3d* valence-band electrons is diagnostic of the oxidation state, where larger ΔBE (binding energy) indicates lower valence states [29]. Fresh MnCe had a ΔBE of 5.27 eV and it increased to 6.42 eV for MnCe-SO_2. In the case of SO_2+H_2O poisoning, it showed a narrow ΔBE of 5.59 eV. Further average oxidation state analysis (AOS, detailed calculation process was exhibited in Fig. S11) showed that the AOS was 3.0, 1.7, and 2.7 for MnCe, MnCe-SO_2, and MnCe-SO_2+H_2O, in line with the change from Mn *2p* analysis. Considering that the reaction atmosphere (NO + O_2 + NH_3) had little effect on the valence of Mn and Ce elements (Fig. S12), the valence change on MnCe catalysts was mainly due to the electron effect from sulfur species. And H_2O significantly affected this interaction between sulfur species and MnCe.

The electronic interaction between sulfur species and active metal sites was disclosed at an atomic level by DFT simulation. According to the previous work [30] and the result of XRD and HR-TEM (Fig. 3**a** and Fig. S13), the CeO_2 (111) crystal plane sliced from a cubic fluorite structure was selected as the surface for investigation (Fig. S14a). MnCe was modeled by substituting one Mn atom with one Ce atom in the surface layer [12]. It was reported that there are abundant oxygen defects formed on Mn-doped CeO_2 catalysts [30]. And this was reflected by the calculated formation energy of an oxygen defect being only 0.09 eV (2.43 eV for CeO_2), indicating the facile formation of defect sites on MnCe catalysts (Fig. S15**)**. As for the influence of H_2O, it was found the dissociation of H_2O on MnCe surface with a defect site was strongly exothermic by −1.95 eV with an energy barrier of only 0.36 eV (Fig. S16), in line with the previous work that H_2O can be easily dissociated on catalyst surface [31,32]. Therefore, the structure of vaporous

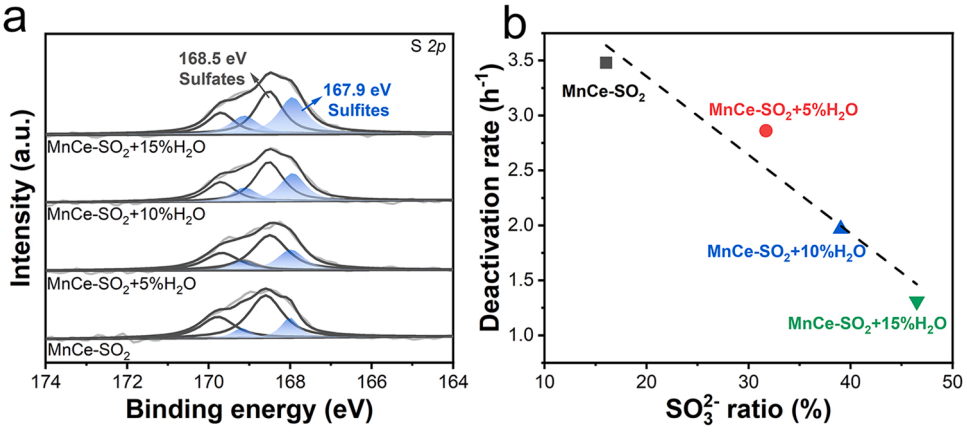

Fig. 4. (a) XPS S *2p* of SO_2 poisoned MnCe with different H_2O content and (b) linear fitting result between surface sulfite ratio and deactivation rate.

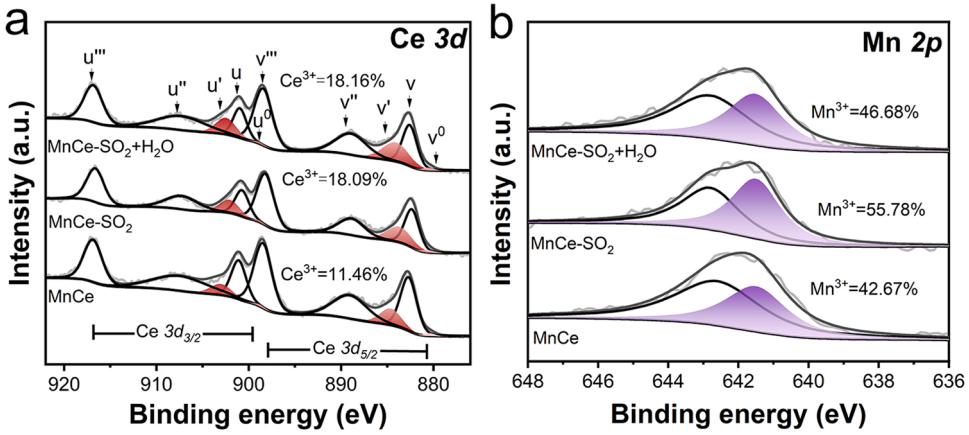

Fig. 5. XPS spectra of (a) Ce *3d* and (b) Mn *2p* over fresh and poisoned MnCe.

water adsorption on MnCe surface was modeled by a dissociated hydroxyl group (Fig. S14c), which was also supported by *in situ* DRIFTS of H_2O adsorption (Fig. S17).

Calculated adsorption geometries of SO_2 on MnCe and MnCe-OH were summarized in Fig. S18**.** The S atom of SO_2 was optimized to bond with the lattice oxygen (Mn-O-Ce) and the hydroxyl group was attached to the defect sites. As shown in Fig. 6a, the S-O band length between SO_2 and surface lattice oxygen on the surface was measured to be 1.54 Å. When the hydroxyl group was introduced, it seemed to have an attractive effect from OH to SO_2 and the S-O (lattice oxygen) band was elongated to 1.63 Å. This result suggests a weakened oxidization property of MnCe to SO_2 [12,33]. Charge density difference was employed to analyze the effect of hydroxyl group on charge distribution. As shown in Fig. 6c-d, the transmission of charge density between S atom and adjacent lattice oxygen was weakened by OH, indicating that surface hydroxyl restricted the electron interaction between sulfur group and MnCe. This result was also reached by Bader charge analysis, which can reflect valence information (Table S4). The Bader charge of S atom over SO_2-MnCe model was simulated to be 2.73 *e*. And it greatly decreased to 2.25 *e* after the introduction of hydroxyl group. The change of Bader charges indicated a lower valence of the surface sulfur species and more sulfites existed over SO_2-MnCe-OH, which was little affected by the adsorption of reactant molecules (NO and NH_3, Fig. S19). This unique effect of hydroxyl on sulfite formation was also confirmed through *in situ* DRIFTS of SO_2 + O_2 adsorption (Fig. S20). Further analysis of Bader charges showed that the hydroxyl group negligibly affected the electron interaction of sulfur species on surface Ce sites (2.37 and 2.36 *e* for SO_2-MnCe and SO_2-MnCe-OH). As a comparison, the disturbance of sulfur species on Mn sites was significantly alleviated by the hydroxyl group and Mn recovered to a higher valence (1.63 and 1.70 *e* for SO_2-MnCe and SO_2-MnCe-OH), in line with the result of XPS (Fig. 5 and S11).

The electronic structures of SO_2-MnCe and SO_2-MnCe-OH were analyzed *via* the partial density of state (PDOS). The spin orbitals of S, Mn, and adjacent Ce atoms were studied and the result was presented in Fig. 7. It shows that the S-*p* spin-up states were hybridized with the Mn-*d* orbital at the conduction band minimum (0.5–1.5 eV), and it shifted to a lower energy region with a band gap increasing from 0.46 eV to 0.91 eV when there presented hydroxyl group, indicating the electron interaction between Mn and S atom became more difficult. Furthermore, the Ce band gap of SO_2-MnCe-OH (2.87 eV) determined from PDOS showed little difference compared to that of SO_2-MnCe (2.92 eV), while the Mn band gap was greatly decreased when introducing the hydroxy group (2.49 eV *vs.* 1.49 eV). As known, the band gap is usually related to reactivity and the active sites with smaller band gap or no gap are more reactive than those with larger ones [34,35]. Therefore, the reactivity of surface Mn sites recovered a lot after the introduction of H_2O. Gevers et. al reported that surface Mn species were the main active sites in SCR reaction and it was not positively affected by surface Ce species in intimate contact, which was just a structural promotor [36]. Therefore, the introduction of H_2O eased the influence of sulfur species on surface active Mn sites and facilitated more sulfite formation, thus alleviating the deactivation of MnCe.

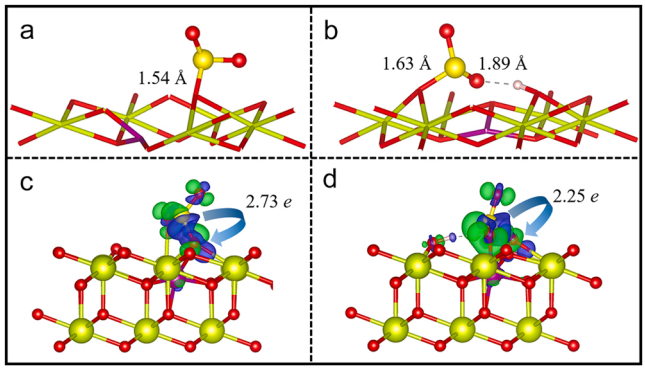

Fig. 6. The optimized structures and corresponding charge density difference at a 0.007 $e{\cdot}Å^{-3}$ isosurface levels of (a, c) SO_2-MnCe and (b, d) SO_2-MnCe-OH. The balls with red, green, purple, yellow, and pink are O, Ce, Mn, S, and H atoms, respectively.

3.5. Redox properties of MnCe catalysts

It was confirmed from the above results that H_2O existence significantly alleviated the electron interaction between surface active Mn sites and sulfur species, thus promoting the formation of more sulfites. To evaluate the effect of distinct sulfur species on redox properties of catalysts, XPS of O *1s*, O_2-TPD, and H_2-TPR were carried out. As shown in Fig. 8a, a relatively faint peak around 531.8 eV and an intense peak around 529.0 eV were observed on pristine MnCe, which was ascribed to the chemisorbed oxygen (O_α) and lattice oxygen (O_β) [37]. After reacting in the stream containing SO_2 and H_2O, the ratio of O_α increased from 34.31% (fresh MnCe) to 51.87% (MnCe-SO_2) and 54.83% (MnCe--SO_2+H_2O). It is generally thought that chemisorbed oxygen is closely related to the redox property and is beneficial for SCR reactions. However, this may not be true for sulfated catalysts because the main contribution of O_α comes from the oxygen in sulfates/sulfites [38]. In addition to the variation of O_α concentration, the binding energies of O_β exhibited an apparent difference. The binding energy of O_β over MnCe-SO_2 (529.7 eV) showed a larger shift to high energy than that over MnCe-SO_2+H_2O (529.5 eV). It is well reported that the S═O band in sulfur species behaves as an electron-withdrawing group [39] and SO_4^{2-}

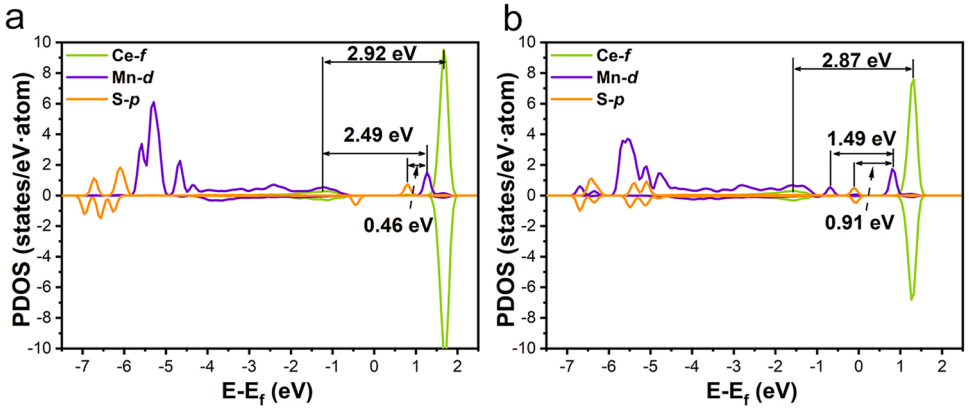

Fig. 7. PDOS of Ce, Mn, and S orbits on the configurations of (a) SO_2-MnCe and (b) SO_2-MnCe-OH.

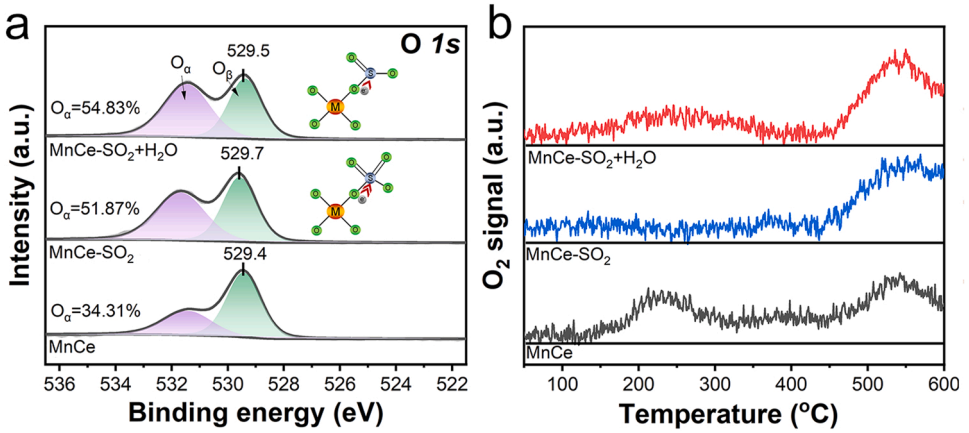

Fig. 8. (a) XPS of O *1s* and (b) O_2-TPD over fresh and poisoned MnCe.

with double S═O bands has a much stronger electron-withdrawing capacity than SO_3^{2-} with only one (Schematic diagram in Fig. 8**a**). Therefore, the observation of smaller binding energy shift of $O_β$ also indicated less disturbance of sulfur species on surface active sites over MnCe--SO_2+H_2O, which supported the result of DFT calculation.

O_2-TPD experiments were further carried out to explore the distinct influence of sulfates and sulfites on surface labile oxygen. As shown in Fig. 8b, for fresh MnCe, desorbed O_2 species below 300 °C were ascribed to active chemisorbed O_2 or active lattice oxygen species on the catalyst surface, and those desorbed within 300–600 °C were attributed to subsurface lattice oxygen [40]. After exposed to SO_2, the peak related to surface active oxygen was no longer present on MnCe-SO_2 with more sulfates, indicating strong interference of sulfates on activating surface oxygen species. As a comparison, MnCe-SO_2+H_2O retained a certain amount of surface O_2 desorption, demonstrating that there existed more active oxygen species and the excellent redox property of MnCe catalysts was partially retained. This result was also supported by H_2-TPR that the reduction signal of Mn species could also be observed on MnCe--SO_2+H_2O with more sulfites, while it could not be detected on MnCe-SO_2 with more sulfates (Fig. S21).

3.6. Adsorption properties of MnCe catalysts

To further explore the effect of diverse sulfur species on the adsorption behavior of reactants (NH_3 and NO_x), the characterizations of NH_3-TPD and NO-TPD were conducted. As shown in Fig. 9a, the acidity of MnCe was significantly enhanced after the SO_2 resistance test. Pristine MnCe only exhibited weak NH_3 adsorption of 0.062 mmol/g. The adsorption capacity of NH_3 increased by nearly 10 times and 4 times, which reached 0.59 mmol/g for MnCe-SO_2 and 0.26 mmol/g for MnCe-SO_2+H_2O. It is worth mentioning that despite the similar amount of adsorbed sulfur species (Table 1), less than half of the NH_3 adsorption was acquired on MnCe-SO_2+H_2O (Table 2). This demonstrates that sulfites might not act as additional acid sites to capture NH_3, probably due to the existence form of sulfite (*e.g.,* metallic sulfites) [41] or the inherent poor acidity of sulfites (Figs. S23-24). When coming to the NO_x-TPD profiles (Fig. 9b), it was found the fresh MnCe showed remarkable NO and NO_2 desorption of 0.21 and 0.22 mmol/g, respectively. As a sharp comparison, little NO and NO_2 desorption could be detected on MnCe-SO_2, suggesting strong competitive adsorption between sulfates and NO_x. However, moderate desorption signals from NO (0.071 mmol/g) and NO_2 (0.021 mmol/g) were still detected over the MnCe-SO_2+H_2O sample, verifying the partial preservation of surface active oxygen species [42].

In situ DRIFTS of reactant adsorption were carried out to deeply distinguish the nature of surface adsorbed species. Fig. 9**c** presented the DRIFTS result of NH_3 adsorption. Several IR vibration bands at 1560, 1428, 1297, 1112, and 1045 cm^{-1} were detected after the adsorption of NH_3 over pristine MnCe. The peaks at 1560, 1297, 1112, and 1045 cm^{-1} could be ascribed to N-H bond vibration from NH_3 adsorbed on Lewis acid sites (LASs) and the band around 1428 cm^{-1} was attributed to NH_4^+ species on Brønsted acid sites (BASs) [1,43]. For MnCe-SO_2, only a strong δ_{as} vibration band of NH_4^+ over BASs at 1436 cm^{-1} appeared and little NH_3 signal over LASs was observed. In contrast, for MnCe--SO_2+H_2O, apart from NH_4^+ on BASs, the peaks at 1112 and 1045 cm^{-1} belonging to the NH_3 adsorption on LASs could still be detected. Considering that the interference of sulfur species on Ce sites was negligibly affected by H_2O, observed LASs could be attributed to

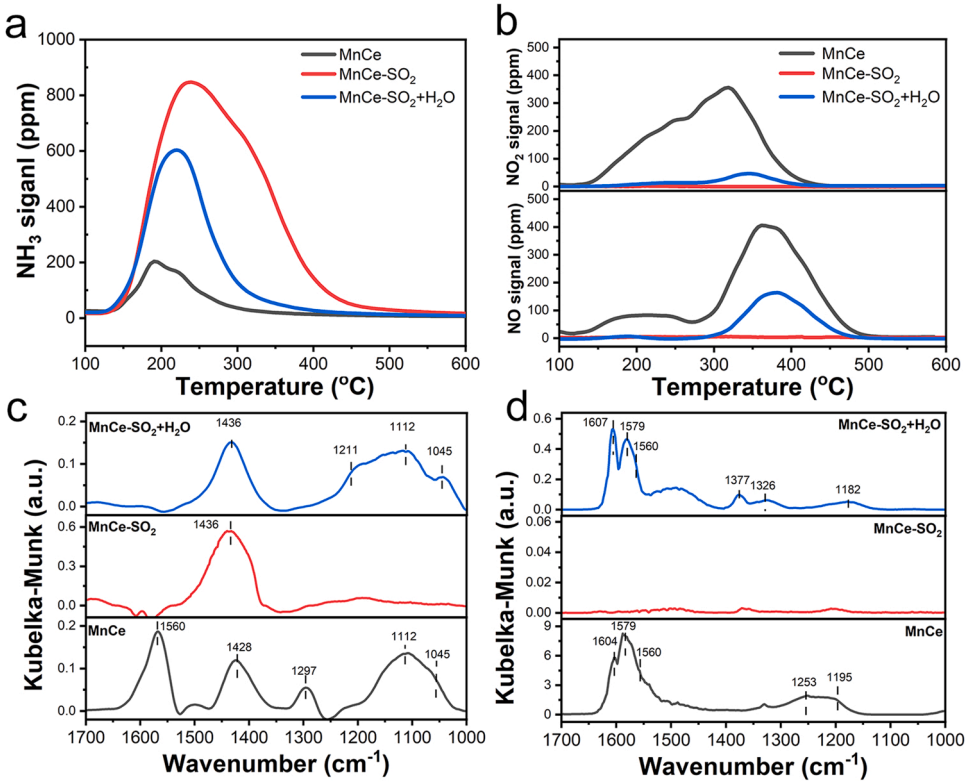

Fig. 9. (a) NH_3-TPD, (b) NO_x-TPD, and *in situ* DRIFTS of (c) NH_3 adsorption and (d) NO_x adsorption over fresh and poisoned MnCe.

Table 2
Quantitative analysis results of NH_3-TPD and NO_x-TPD over fresh and poisoned MnCe catalysts.

Sample	Desorption amount (mmol/g)		
	NH_3	NO	NO_2
MnCe	0.062	0.21	0.22
MnCe-SO_2	0.59	0	0
MnCe-SO_2+H_2O	0.26	0.071	0.021

retained acid sites on Mn sites due to minor disturbance of sulfites. Moreover, a new band attributing to δ_s vibration modes of NH_3 on LASs at 1211 cm^{-1} was detected, suggesting the unique effect of sulfites in inducing the formation of LASs on Mn sites [8].

Fig. 9d showed DRIFT spectra of NO + O_2 adsorption on MnCe. After the exposure to NO + O_2 at 100 °C, diverse IR bands belonging to monodentate nitrates (1560 and 1256 cm^{-1}), bidentate nitrates (1579 cm^{-1}), and bridging nitrates (1604 and 1204 cm^{-1}) emerged over fresh MnCe [21,44,45]. It is seen that after the SO_2 resistance test under a dry state, the NO_x adsorption was totally suppressed by surface sulfates. Even though the scales were 150 times in difference, almost no nitrates/nitrites signals could be observed, which supported the result of NO_x-TPD. As for MnCe-SO_2+H_2O, less influence of sulfites on NO_x adsorption was displayed. It is clear that several bands attributed to monodentate nitrates, bidentate nitrates, and bridging nitrates could still be detected, which were probably bound to Mn sites. Besides, two new vibration peaks at 1378 and 1334 cm^{-1} belonging to bidentate nitro and cis-$N_2O_2^{2-}$ with high reactivity were detected, which was expected to make contribution to the restricted deactivation in NH_3-SCR [46,47].

Based on the TPD and DRIFTS results, the influences of sulfates and sulfites on NH_3 and NO_x adsorption were revealed. Abundant LASs were obtained on pristine MnCe and they were totally lost due to the formation of sulfates, resulting in the exclusive presence of BASs on MnCe-SO_2. Besides, the strong competitive adsorption between sulfates and NO_x species made it difficult to adsorb NO_x, which could hinder the occurrence of SCR reaction *via* Langmuir-Hinshelwood (L-H) mechanism. In contrast, sulfites exhibited less influence on the adsorption properties of active Mn sites and even promoted the formation of new LASs. Furthermore, appropriate electron interaction also induced the formation of surface nitrite species on Mn sites, which are generally thought to be much more active than nitrates. To confirm the reactivity of surface adsorbed species, a reaction mechanism study was carried out.

3.7. Reaction mechanism analysis

To gain insight into the influence of diverse sulfur species on the NO_x reduction mechanism, time-resolved *in situ* DRIFTS of transient reaction was performed over MnCe-SO_2 and MnCe-SO_2+H_2O. The evolution of surface ammonia species under NO + O_2 was first explored and the result was presented in Fig. 10. For MnCe-SO_2 with abundant sulfates, after NH_3 adsorption and N_2 purge, almost all the LASs was occupied by sulfates and only infrared bands characteristics of NH_4^+ over BASs emerged. It was gradually consumed after the injection of NO + O_2 and little nitrate species could be detected, indicating the dominant occurrence of Eley-Rideal (E-R) reaction route over MnCe-SO_2. As a comparison, reserved NH_3 on Mn sites (LASs) in the MnCe-SO_2+H_2O sample exhibited a preferential tendency to react with NO, which was quickly consumed in the first 7 min. After that, NH_4^+ over BASs started to react. The relative reaction rates of NH_3 at different sites were exhibited in Fig. 10c and the reactivity of NH_3 on pristine MnCe was also provided for comparison (Fig. S25). For both MnCe-SO_2 and MnCe-SO_2+H_2O, the reaction rate of NH_4^+ was calculated to be 0.10 min^{-1}, indicating that NH_4^+ over sulfates had a similar reactivity ability. However, for NH_3 over LASs, in addition to preferential reaction ability, the relative reaction rate over MnCe-SO_2+H_2O was calculated to be 0.15 min^{-1}. This value was comparable to the NH_3 reaction rate of fresh MnCe and 50% larger than NH_4^+ over surface sulfates, indicating the excellent reaction ability of retained NH_3 over LASs at low temperatures.

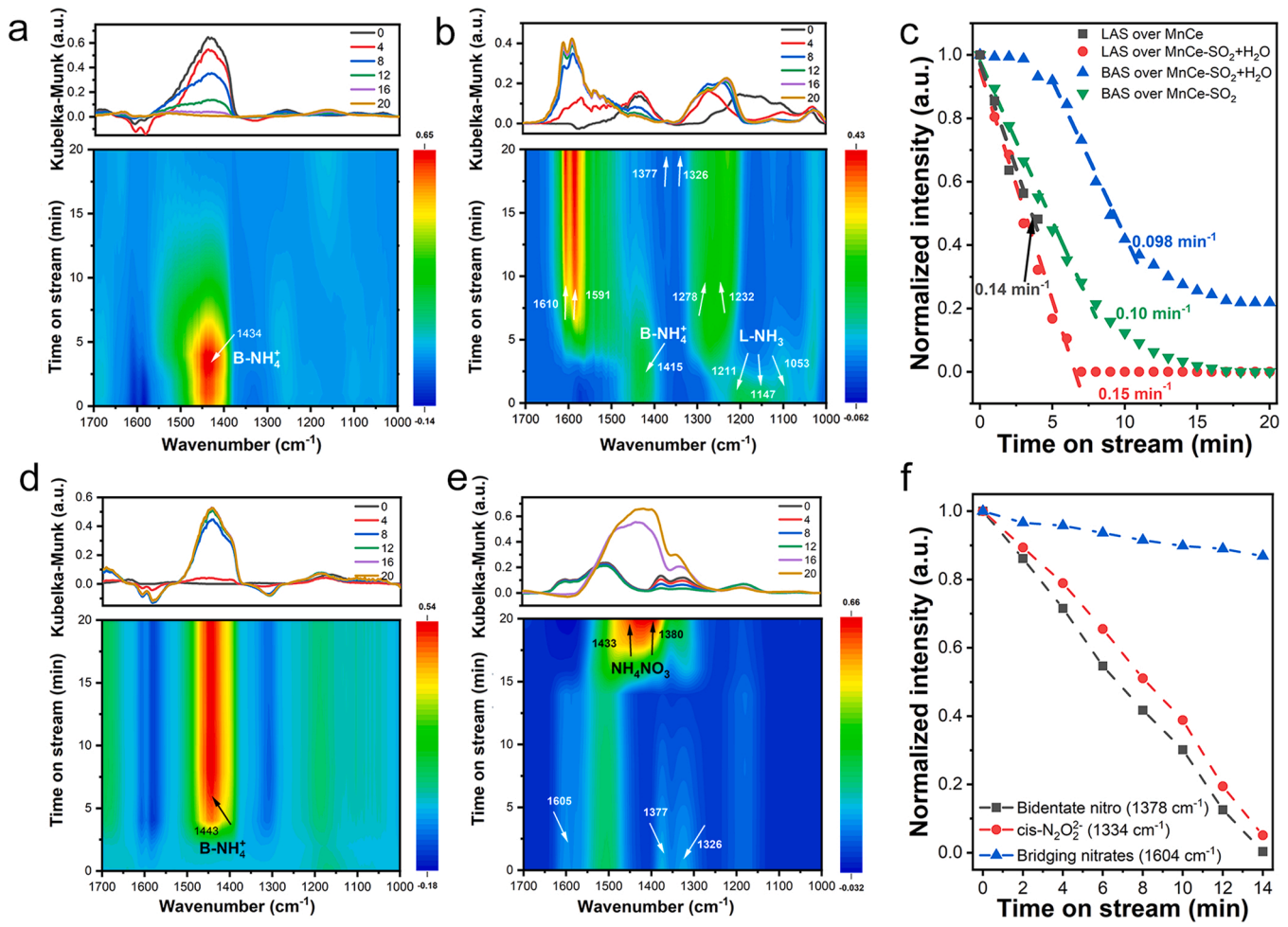

Fig. 10. Time-revolved *in situ* DRIFTS of (a, b) NO + O_2 reaction with pre-adsorbed NH_3 and (d, e) NH_3 reaction with pre-adsorbed NO + O_2 over MnCe-SO_2 and MnCe-SO_2+H_2O, respectively; Normalized intensity of adsorbed (c) NH_3 and (f) NO_x signal as a function of time.

The *in situ* DRIFTS result of NH_3 reaction with pre-adsorbed NO_x was presented in Fig. 10d. Little nitrates could be detected after being exposed to NO + O_2 stream over MnCe-SO_2, and the introduced NH_3 could only exist as NH_4^+ species over BASs. For MnCe-SO_2+H_2O, compared with NO + O_2 adsorption, the intensity of some nitrate species decreased a lot after the N_2 purge. Nevertheless, the typical signals from nitrates (1605, 1580, 1560, and 1182 cm^{-1}), bidentate nitro (1378 cm^{-1}), and cis-$N_2O_2^{2-}$ (1334 cm^{-1}) over Mn sites were still preserved. It is clear to see that bidentate nitro and cis-$N_2O_2^{2-}$ were completely consumed in 14 min (Fig. 10e-f). The nitrates remained stable in the first 14 min and they changed significantly after the nitrites were totally reduced. After that, the peaks at 1603 cm^{-1} disappeared rapidly and the signal ascribed to NH_4NO_3 appeared (1430 and 1380 cm^{-1}), in line with that over fresh MnCe (Fig. S26). Therefore, we can conclude that both nitrates and nitrites participated in the surface reaction over MnCe-SO_2+H_2O.

The kinetics reaction order test was carried out to further disclose the reaction mechanism. Busca et al. summarized that SCR reaction follows

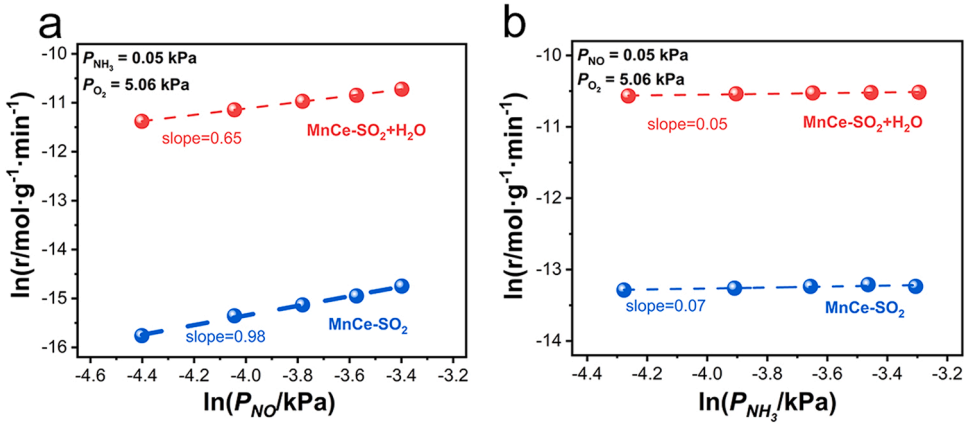

Fig. 11. The dependence of NO_x reduction rate on the partial pressure of (a) NO and (b) NH_3 over poisoned catalysts at 100 °C.

zero-order dependence with O_2 when O_2 content exceeds 1 *vol.*% (5 *vol.*% in this work) [48]. Therefore, based on the collected experimental data shown in Fig. 11, the kinetic equation can be expressed as the following:

$$r_{MnCe-SO_2} = k_{MnCe-SO_2}[NO]^{0.98}[NH_3]^{0.07}$$

$$r_{MnCe-SO_2+H_2O} = k_{MnCe-SO_2+H_2O}[NO]^{0.65}[NH_3]^{0.05}$$

From the above equations, it is known both L-H and E-R mechanisms occurred on fresh MnCe (Fig. S27). After SO_2 poisoning, the order of NO on MnCe-SO_2 went up to close to 1, suggesting that the reaction rate was proportional to the partial pressure of gaseous NO. Combined with the results of TPD and *in situ* DRIFTS, it can be deduced that the L-H mechanism of MnCe was cut off by sulfate species and only gaseous NO took part in the reaction. For MnCe-SO_2+H_2O, sulfite species displayed less disturbance to the adsorptions of NH_3 and NO_x over Mn sites. The reaction order of NO was tested to be 0.65, far smaller than 1. Thus, NO could participate in the catalytic reaction in gaseous form along with surface adsorbed NO_x species [49]. Both L-H and E-R mechanisms contributed to the NO elimination on MnCe-SO_2+H_2O, which was in line with the result of calculated kinetic parameters result (Fig. S28). As for the NH_3 reaction order, it was all close to zero for poisoned catalysts, indicating that NH_3 mainly participated in the reaction through the form of adsorbed ammonia species.

On the basis of the structure properties analysis and reaction mechanism study, distinct effects of sulfates and sulfites over MnCe catalysts at ultra-low temperature were deduced and summarized (Scheme 1). The surface of MnCe-SO_2 was mainly covered by sulfate species, which limited the redox capacity and significantly hindered the adsorptions of NH_3 over LASs and NO_x over both surface Ce and Mn sites. Only the E-R mechanism involving NH_4^+ anchored on BASs (sulfate species) occurred over MnCe-SO_2, resulting in poor catalytic performance in the presence of SO_2. As for MnCe-SO_2+H_2O, dissociated hydroxyl from H_2O at defect sites greatly alleviated electron transfer between sulfur species and active Mn sites, thus inhibiting the oxidation of sulfites and protecting the active Mn sites. The sulfite species retained the NH_3 adsorption on LASs, which exhibited a 50% faster reaction rate than NH_4^+ provided by sulfates. Furthermore, sulfites induced the formation of ad-NO_x species with higher reactivity (bidentate nitro and cis-$N_2O_2^{2-}$). Thus, the reaction followed both E-R and L-H mechanisms on MnCe-SO_2+H_2O.

3.8. Implication of the study

Owing to the ubiquitous presence of SO_2 and H_2O in exhaust gases involving NO, extensive studies have been operated to explore the reaction behavior and poisoning mechanism of SCR catalysts under SO_2 + H_2O conditions. It is well recognized that SCR catalysts undergo severe deactivation when exposed to SO_2, and H_2O addition can accelerate this process. However, these previous works mainly focused on the temperature above 150 °C. At that reaction condition, the surface sulfur species are dominated by sulfates, either in the form of metal sulfates or NH_4HSO_4. Both species can disrupt the redox property or block the active sites of SCR catalysts *via* chemical bonding and physical deposition.

Actually, in some studies regarding SO_2 oxidation, it is found that redox catalysts show a limited ability to oxidize SO_2 when the operating temperature is lower than 150 °C. There are plenty of sulfites that existed on the catalyst surface [2,50]. And such fundamental questions like the factors influencing sulfite formation and how sulfites affect SCR catalysts still lack a comprehensive understanding in the denitration reaction. In the present study, based on the analysis results from IC and XPS, we confirm the existence of sulfite species, which is promoted with the assistance of H_2O at ultra-low temperatures. And the experiment result clearly shows that SO_2 resistance of catalysts under humid conditions at such temperature is completely reversed with that at a higher temperature of 200 °C (Fig. S7), indicating the distinct effects of sulfates and sulfites on SCR catalysts. Specifically, sulfates can provide additional BASs for NH_4^+ adsorption, but it greatly affects the surface oxygen activation and occupies adsorption of active species. As a sharp comparison, sulfites act more like a promotor, which induced the formation of more active adsorbed species (*e.g.,* nitrites and new LASs). Hence, by referring to the literature, the result of this study confirms the formation of sulfites at ultra-low temperatures and reveals the unique properties of sulfites on the catalytic performance and SO_2 resistance of SCR catalysts.

4. Conclusion

In conclusion, we proposed in the present study a detailed mechanism of H_2O promotion on the SO_2 tolerance of MnCe catalyst working at ultra-low temperature (100 °C). It was revealed that the effect of H_2O on SO_2 tolerance actually exerted a temperature-dependent feature and at the temperature as low as 100 °C, H_2O exhibited negligible impact on the accumulation of sulfur species on the catalyst surface. Instead, it apparently affected the distribution of sulfur species (*i.e.,* sulfites and sulfates). The generation of hydroxyl species through H_2O disassociation facilitated more sulfite species formation by restricting the electron interaction between sulfur species and active Mn sites. Compared to sulfates providing more stronger BASs and limiting the redox property of catalysts, sulfite species did not act as additional acid sites but preserved surface LASs and induced the formation of nitrites with high reactivity in SCR reaction. Thus, both L-H and E-R mechanisms contributed to the enhanced catalytic performance of MnCe under SO_2 and H_2O coexistence.

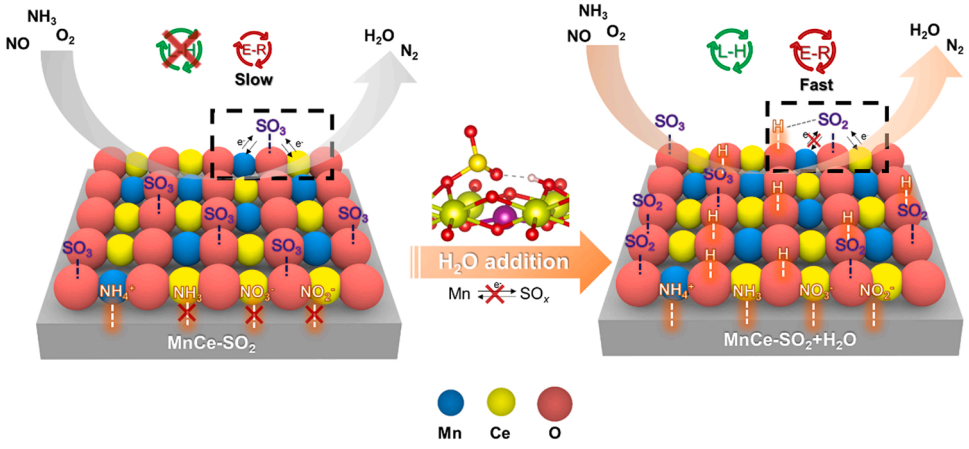

Scheme 1. Distinct influence of sulfate and sulfite species on adsorption properties and reaction mechanism over MnO_x-CeO_2 catalysts.

CRediT authorship contribution statement

Jiawei Ji: Conceptualization, Data curation, Methodology, Validation, Investigation, Writing - original draft, Formal analysis, Visualization, **Ningze Gao:** Investigation, Data curation, Formal analysis, Visualization, **Wang Song:** Investigation, Visualization, Resources,. **Yu Tang:** Data curation, Investigation, Formal analysis, **Yandi Cai:** Data curation, Validation, **Li Han:** Investigation, **Lijun Cheng:** Investigation, Formal analysis, **Jingfang Sun:** Investigation, Supervision, **Shenggui Ma:** Methodology, Data curation, Formal analysis, Visualization,. **Yinghao Chu:** Resources, Investigation, **Changjin Tang:** Conceptualization, Formal analysis, Funding acquisition, Project administration, Resources, Supervision, Writing - review & editing, **Lin Dong:** Funding acquisition, Sources, Supervision, Writing - review & editing.

Declaration of Competing Interest

The authors declare that they have no known competing financial interests or personal relationships that could have appeared to influence the work reported in this paper.

Data Availability

No data was used for the research described in the article.

Acknowledgments

The financial supports from the National Science Foundation of China (21976081, 21972062, 22272077, 22276097) and the Major Scientific and Technological Project of Bingtuan (2018AA002), are acknowledged.

Supplementary Materials

Relevant information regarding detailed reaction conditions reported in the references; ion concentration from IC; external and internal diffusion elimination; SO_2 resistance; EDS-mapping; XPS; HR-TEM; optimized structures; calculated adsorption geometries; dissociation pathway of H_2O; H_2-TPR; *in situ* DRIFTS; NH_3-TPD; reaction order test; kinetic parameter calculation.

Appendix A. Supporting information

Supplementary data associated with this article can be found in the online version at doi:10.1016/j.apcatb.2022.122263.

References

[1] A. Marberger, D. Ferri, M. Elsener, O. Krocher, The significance of lewis acid sites for the selective catalytic reduction of nitric oxide on vanadium-based catalysts, Angew. Chem. Int. Ed. 55 (2016) 11989–11994.
[2] J. Kim, D. Kim, J. Park, K. Jeong, H. Ha, Decrypting catalytic NO_x activation and poison fragmentation routes boosted by mono- and bi-dentate surface SO_3^{2-}/SO_4^{2-} modifiers under a SO_2-containing flue gas stream, ACS Catal. 12 (2022) 2086–2107.
[3] R. Nuguid, D. Ferri, A. Marberger, M. Nachtegaal, O. Kröcher, Modulated excitation raman spectroscopy of V_2O_5/TiO_2: mechanistic insights into the selective catalytic reduction of NO with NH_3, ACS Catal. 9 (2019) 6814–6820.
[4] X. Zhao, L. Huang, H. Li, H. Hu, X. Hu, L. Shi, D. Zhang, Promotional effects of zirconium doped $CeVO_4$ for the low-temperature selective catalytic reduction of NO_x with NH_3, Appl. Catal. B 183 (2016) 269–281.
[5] B. Jia, J. Guo, H. Luo, S. Shu, N. Fang, J. Li, Study of NO removal and resistance to SO_2 and H_2O of MnO/TiO_2, MnO/ZrO_2 and MnO/ZrO_2-TiO_2, Appl. Catal. A 553 (2018) 82–90.
[6] K. Guo, J. Ji, W. Song, J. Sun, C. Tang, L. Dong, Conquering ammonium bisulfate poison over low-temperature NH_3-SCR catalysts: a critical review, Appl. Catal. B 297 (2021), 120388.
[7] F. Wang, P. Wang, T. Lan, Y. Shen, W. Ren, D. Zhang, Ultralow-temperature NO_x reduction over $SmMn_2O_5$ mullite catalysts via modulating the superficial dual-functional active sites, ACS Catal. 12 (2022) 7622–7632.
[8] R. Xie, L. Ma, Z. Li, Z. Qu, N. Yan, J. Li, Review of sulfur promotion effects on metal oxide catalysts for NO_x emission control, ACS Catal. 11 (2021) 13119–13139.
[9] L. Xu, C. Wang, H. Chang, Q. Wu, T. Zhang, J. Li, New insight into SO_2 poisoning and regeneration of CeO_2-WO_3/TiO_2 and V_2O_5-WO_3/TiO_2 catalysts for low-temperature NH_3-SCR, Environ. Sci. Technol. 52 (2018) 7064–7071.
[10] R. Gui, Q. Yan, T. Xue, Y. Gao, Y. Li, T. Zhu, Q. Wang, The promoting/inhibiting effect of water vapor on the selective catalytic reduction of NO_x, J. Hazard. Mater. 439 (2022), 129665.
[11] W. Kijlstra, J. Daamen, J. vandeGraaf, B. vanderLinden, E. Poels, A. Bliek, Inhibiting and deactivating effects of water on the selective catalytic reduction of nitric oxide with ammonia over MnO_x/Al_2O_3, Appl. Catal. B 7 (1996) 337–357.
[12] X. Fang, Y. Liu, Y. Cheng, W. Cen, Mechanism of Ce-modified birnessite-MnO_2 in promoting SO_2 poisoning resistance for low-temperature NH_3-SCR, ACS Catal. 11 (2021) 4125–4135.
[13] G. Kresse, J. Furthmuller, Efficient iterative schemes for ab initio total-energy calculations using a plane-wave basis set, Phys. Rev. B 54 (1996) 11169–11186.
[14] D. García Pintos, A. Juan, B. Irigoyen, Mn-doped CeO_2: DFT+U study of a catalyst for oxidation reactions, J. Phys. Chem. C 117 (2013) 18063–18073.
[15] G. Qi, R. Yang, R. Chang, MnO_x-CeO_2 mixed oxides prepared by co-precipitation for selective catalytic reduction of NO with NH_3 at low temperatures, Appl. Catal. B 51 (2004) 93–106.
[16] Z. Lei, B. Han, K. Yang, B. Chen, Influence of H_2O on the low-temperature NH_3-SCR of NO over V_2O_5/AC catalyst: an experimental and modeling study, Chem. Eng. J. 215–216 (2013) 651–657.
[17] F. Liu, H. He, Selective catalytic reduction of NO with NH_3 over manganese substituted iron titanate catalyst: reaction mechanism and H_2O/SO_2 inhibition mechanism study, Catal. Today 153 (2010) 70–76.
[18] S. Xiong, Y. Liao, X. Xiao, H. Dang, S. Yang, The mechanism of the effect of H_2O on the low temperature selective catalytic reduction of NO with NH_3 over Mn-Fe spinel, Catal. Sci. Technol. 5 (2015) 2132–2140.
[19] F. Liu, H. He, Z. Lian, W. Shan, L. Xie, K. Asakura, W. Yang, H. Deng, Highly dispersed iron vanadate catalyst supported on TiO_2 for the selective catalytic reduction of NO_x with NH_3, J. Catal. 307 (2013) 340–351.
[20] Z. Huang, Z. Zhu, Z. Liu, Q. Liu, Formation and reaction of ammonium sulfate salts on V_2O_5/AC catalyst during selective catalytic reduction of nitric oxide by ammonia at low temperatures, J. Catal. 214 (2003) 213–219.
[21] S. Yang, Y. Guo, H. Chang, L. Ma, Y. Peng, Z. Qu, N. Yan, C. Wang, J. Li, Novel effect of SO_2 on the SCR reaction over CeO_2: Mechanism and significance, Appl. Catal., B 136–137 (2013) 19–28.
[22] W. Tan, J. Wang, L. Li, A. Liu, G. Song, K. Guo, Y. Luo, F. Liu, F. Gao, L. Dong, Gas phase sulfation of ceria-zirconia solid solutions for generating highly efficient and SO_2 resistant NH_3-SCR catalysts for NO removal, J. Hazard. Mater. 388 (2020).
[23] K. Wijayanti, K. Xie, A. Kumar, K. Kamasamudram, L. Olsson, Effect of gas compositions on SO_2 poisoning over Cu/SSZ-13 used for NH_3-SCR, Appl. Catal., B 219 (2017) 142–154.
[24] E. Romano, K. Schulz, A. XPS, investigation of SO_2 adsorption on ceria-zirconia mixed-metal oxides, Appl. Surf. Sci. 246 (2005) 262–270.
[25] X. Wang, X. Du, S. Liu, G. Yang, Y. Chen, L. Zhang, X. Tu, Understanding the deposition and reaction mechanism of ammonium bisulfate on a vanadia SCR catalyst: a combined DFT and experimental study, Appl. Catal., B 260 (2020), 118168.
[26] S. Yu, Y. Lu, Y. Cao, J. Wang, B. Sun, F. Gao, C. Tang, L. Dong, Composite catalytic systems: a strategy for developing the low temperature NH_3-SCR catalysts with satisfactory SO_2 and H_2O tolerance, Catal. Today 327 (2019) 235–245.
[27] A. Pfau, K. Schierbaum, The electronic-structure of stoichiometric and reduced CeO_2 surfaces - an XPS, UPS and HREELS study, Sur. Sci 321 (1994) 71–80.
[28] P. Sudarsanam, B. Hillary, M. Amin, S. Hamid, S. Bhargava, Structure-activity relationships of nanoscale MnO_x/CeO_2 heterostructured catalysts for selective oxidation of amines under eco-friendly conditions, Appl. Catal. B 185 (2016) 213–224.
[29] M. Biesinger, B. Payne, A. Grosvenor, L. Lau, A. Gerson, R. Smart, Resolving surface chemical states in XPS analysis of first row transition metals, oxides and hydroxides: Cr, Mn, Fe, Co and Ni, Appl. Surf. Sci. 257 (2011) 2717–2730.
[30] L. Ye, P. Lu, X. Chen, P. Fang, Y. Peng, J. Li, H. Huang, The deactivation mechanism of toluene on MnO_x-CeO_2 SCR catalyst, Appl. Catal., B 277 (2020), 119257.
[31] H. Hansen, C. Wolverton, Kinetics and thermodynamics of H_2O dissociation on reduced $CeO_2(111)$, J. Phys. Chem. C 118 (2014) 27402–27414.
[32] H. Zhang, K. Zhao, Y. Gao, Y. Tian, P. Liang, Inhibitory effects of water vapor on elemental mercury removal performance over cerium-oxide-modified semi-coke, Chem. Eng. J. 324 (2017) 279–286.
[33] A. Dey, T. Okamura, N. Ueyama, B. Hedman, K. Hodgson, E. Solomon, Sulfur K-edge XAS and DFT calculations on P450 model complexes: Effects of hydrogen bonding on electronic structure and redox potentials, J. Am. Chem. Soc. 127 (2005) 12046–12053.
[34] Y. Peng, J. Li, W. Si, X. Li, W. Shi, J. Luo, J. Fu, J. Crittenden, J. Hao, Ceria promotion on the potassium resistance of MnO_x/TiO_2 SCR catalysts: an experimental and DFT study, Chem. Eng. J. 269 (2015) 44–50.
[35] M. Calatayud, B. Mguig, C. Minot, A DFT study on the hydrated V_2O_5-TiO_2-anatase catalyst: stability of monomeric species, Theor. Chem. Acc. 114 (2005) 29–37.
[36] L. Gevers, L. Enakonda, A. Shahid, S. Ould-Chikh, C. Silva, P. Paalanen, A. Aguilar-Tapia, J. Hazemann, M. Hedhili, F. Wen, J. Ruiz-Martinez, Unraveling the structure and role of Mn and Ce for NO_x reduction in application-relevant catalysts, Nat. Commun. 13 (2022) 2960.

[37] A. Ramírez, P. Hillebrand, D. Stellmach, M. May, P. Bogdanoff, S. Fiechter, Evaluation of MnO_x, Mn_2O_3, and Mn_3O_4 electrodeposited films for the oxygen evolution reaction of water, J. Phys. Chem. C 118 (2014) 14073–14081.
[38] Q. Wu, X. Chen, J. Mi, S. Cai, L. Ma, W. Zhao, J. Chen, J. Li, The Absence of oxygen in sulfation promotes the performance of the sulfated CeO_2 catalyst for low-temperature selective catalytic reduction of NO_x by NH_3: Redox property versus acidity, ACS Sustain. Chem. Eng. 9 (2021) 967–979.
[39] R. Paul, J. Puri, K. Malhotra, Behaviour of compounds containing sulphur-oxygen bond in disulphuric acid, J. Inorg. Nucl. Chem. 33 (1971) 2459–2467.
[40] W. Yang, Z. Su, Z. Xu, W. Yang, Y. Peng, J. Li, Comparative study of α-, β-, γ- and δ-MnO_2 on toluene oxidation: Oxygen vacancies and reaction intermediates, Appl. Catal., B 260 (2020), 118150.
[41] L. Chen, V. Agrawal, S. Tait, Sulfate promotion of selective catalytic reduction of nitric oxide by ammonia on ceria, Catal. Sci. Technol. 9 (2019) 1802–1815.
[42] J. Hwang, R. Rao, L. Giordano, K. Akkiraju, X. Wang, E. Crumlin, H. Bluhm, Y. Shao-Horn, Regulating oxygen activity of perovskites to promote NO_x oxidation and reduction kinetics, Nat. Catal. 4 (2021) 663–673.
[43] K. Lee, P. Kumar, M. Maqbool, K. Rao, K. Song, H. Ha, Ceria added Sb-V_2O_5/TiO_2 catalysts for low temperature NH_3-SCR: Physico-chemical properties and catalytic activity, Appl. Catal. B 142 (2013) 705–717.
[44] X. Yao, R. Zhao, L. Chen, J. Du, C. Tao, F. Yang, L. Dong, Selective catalytic reduction of NO_x by NH_3 over CeO_2 supported on TiO_2: Comparison of anatase, brookite, and rutile, Appl. Catal. B 208 (2017) 82–93.
[45] J. Ji, Y. Tang, L. Han, P. Ran, W. Song, Y. Cai, W. Tan, J. Sun, C. Tang, L. Dong, Cerium manganese oxides coupled with ZSM-5: a novel SCR catalyst with superior K resistance, Chem. Eng. J. 445 (2022).
[46] K. Hadjiivanov, Identification of neutral and charged N_xO_y surface species by IR spectroscopy, Catal. Rev. 42 (2000) 71–144.
[47] J. Ji, M. Jing, X. Wang, W. Tan, K. Guo, L. Li, X. Wang, W. Song, L. Cheng, J. Sun, W. Song, C. Tang, J. Liu, L. Dong, Activating low-temperature NH_3-SCR catalyst by breaking the strong interface between acid and redox sites: a case of model $Ce_2(SO_4)_3$-CeO_2 study, J. Catal. 399 (2021) 212–223.
[48] G. Busca, L. Lietti, G. Ramis, F. Berti, Chemical and mechanistic aspects of the selective catalytic reduction of NO_x by ammonia over oxide catalysts: a review, Appl. Catal. B 18 (1998) 1–36.
[49] S. Xie, W. Tan, Y. Li, L. Ma, S. Ehrlich, J. Deng, P. Xu, F. Gao, L. Dong, F. Liu, Copper single atom-triggered niobia-ceria catalyst for efficient low-temperature reduction of nitrogen oxides, ACS Catal. 12 (2022) 2441–2453.
[50] M. Wilburn, W. Epling, Formation and decomposition of sulfite and sulfate species on Pt/Pd catalysts: an SO_2 oxidation and sulfur exposure study, ACS Catal. 9 (2019) 640–648.